Journal of Quantitative Spectroscopy & Radiative Transfer 232 (2019) 152–155

Contents lists available at ScienceDirect

Journal of Quantitative Spectroscopy & Radiative Transfer

journal homepage: www.elsevier.com/locate/jqsrt

# Flexible metalized tubes for electromagnetic waveguiding

Dmitry Filonov[a,c,*], Hahi Barhom[a], Andrey Shmidt[a], Yelena Sverdlov[a], Yosi Shacham-Diamand[a], Amir Boag[a], Pavel Ginzburg[a,b]

[a] School of Electrical Engineering, Tel Aviv University, Tel Aviv 69978, Israel
[b] Light-Matter Interaction Centre, Tel Aviv University, Tel Aviv 69978, Israel
[c] Department of Nanophotonics and Metamaterials, ITMO University, St-Petersburg 197101, Russia

ARTICLE INFO

*Article history:*
Received 19 March 2019
Revised 26 April 2019
Accepted 7 May 2019
Available online 8 May 2019

ABSTRACT

Low loss electromagnetic energy transport over long distances motivates the development of different types of waveguiding systems. Requirements of high quality optically polished waveguide surfaces needed in high-frequency applications and low-cost manufacturing are practically incompatible in current realizations. Here we demonstrate a new paradigm solution, based on surface functionalization with subsequent electroless plating of conductive micron smooth copper layer on the inner surface of flexible non-conducting poly-carbonate tubes. The structure was shown to support reasonable guiding performances ($\sim 5 \cdot 10^{-3}$ cm$^{-1}$) at Ku-band. The mechanically flexible design of the system allows shaping the waveguide network almost on demand. In particular, an efficient energy guiding over a closed loop with 8 lambda radius was demonstrated. The new platform of high quality metalized flexible waveguiding systems opens new opportunities in designs of cheap and efficient networks, operating over a broad spectral range, approaching tens of GHz and even higher.



## 1. Introduction

Efficient transport of electromagnetic energy over distances requires the development of different types of waveguiding systems. Many architectures have been demonstrated over the years and each one provides solutions for a specific frequency range and related applications [1]. Minimization of propagation and bending losses along with integrability within larger-scale devices are among the key parameters, required from efficient interconnecting systems. Losses become a critical factor, affecting the performance of millimeter wave devices. Interface roughness on the level of optically polished high-quality surfaces is required from the implementations. As a result, the overall prices and bulky realizations of waveguiding components become a significant factor. Minimization of bending losses can be achieved by exploiting geometries, where electromagnetic radiation is enclosed within a confined volume. Typical representative examples here include rectangular and circular/elliptical geometries. Furthermore, the guided mode in those structures is confined in a void and, as a result, propagation losses are minimized (especially, if the core is vacuumed). Though some commercial solutions are available, bending of enclosed waveguides, is quite a complex technological challenge, as the millimeter-size aperture (Ka-band and higher) should be maintained along the entire curved trajectory.

One among probable recent solutions, which allows constructing quite complex geometries, utilizes recent capabilities of additive manufacturing. Metallization of plastic components is fast developing technological direction, as it can provide significant advantages over conventional realizations in geometric flexibility. Several successful demonstrations of this approach include 3D printed metalized waveguide filters [2], waveguiding systems and related components [3,4] (also for high GHz-THz and without metallization [5,6]), antenna devices and components [7–9], and others [10]. Furthermore, it is worth mentioning other additive manufacturing techniques, which allow the production of high-quality RF components, with an emphasis on antenna devices [11]. Different types of antennas, fabricated with CNC milling technique [12,13], Laser Direct Structuring [14–16], conformal printing of metallic inks [17], conductive inkjet printing [18], ultrasonic wire mesh embedding [19], and metal deposition trough a mask on a curve surface [20,21], selective polymer metallization [22] were reported. Furthermore, integration of 3D printed plastic materials within antenna designs was demonstrated (e.g. [23,24]) and fabrication of low-profile devices with several materials has been shown [25].

In general, three main advantages of 3D printed polymers-based structures can be identified. The first one is their lightweights in comparison with solid metal made counterparts. Since only a thin conductive layer (skin depth of several microns for high

* Corresponding author.
*E-mail address:* dmitriif@mail.tau.ac.il (D. Filonov).

https://doi.org/10.1016/j.jqsrt.2019.05.008
0022-4073/

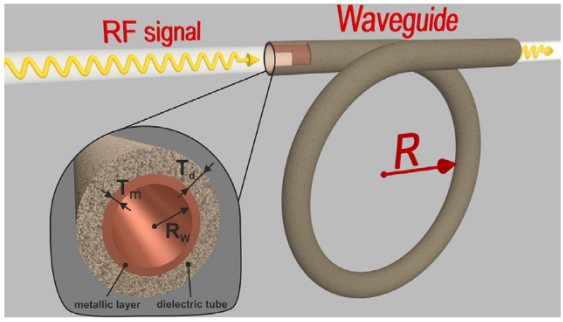


**Fig. 1.** Schematics of a metalized bendable dielectric tube for high frequency waveguiding applications.

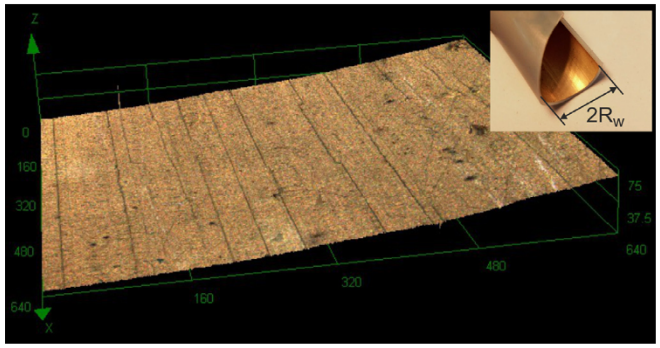


**Fig. 2.** Surface profile of 2.5 mm × 1 mm section of a metalized tube. (Inset) Photograph of the cut section of the tube.

GHz frequencies, if conventional metals are in use) is required for providing efficient waveguiding properties, lightweight polymers can serve as bulk rigid materials, supporting the structure. The second advantage of metalized 3D-printing approach to waveguiding systems is their potential flexibility to provide quite complex geometries (e.g. complex 3D networks, power divides, and others), which are hard to obtain with conventional milling techniques. It is worth noting that rigid 3D structures, once being fabricated, cannot be reshaped. Our proposal, however, is lacking of these limitations. The last and already mentioned factor is the manufacturing cost, which can be significantly reduced in the case when additive manufacturing techniques are in use.

Here we demonstrate a new waveguiding system, based on metallization of flexible polymer tubes (Fig. 1). The distinctive advantages of this architecture include its extremely low cost and mechanical flexibility. Inner surfaces of initially bendable polymer tubes are metalized with an electroless plating technique and, as a result, high-quality RF conductivity is achieved. Furthermore, controllable chemical deposition process was demonstrated to provide high-quality metallization layers with micron-scale roughness along centimeter-range tube cross-sections. Mechanical flexibility of the tube waveguides allows bending them almost on demand without requiring an a priori knowledge of a layout of an end-user.

The Letter is organized as follows: basic technological principles of the metallization are discussed first and then followed by experimental demonstration of the new system and its performance, analyzed with resonant Fabry-Perot-based methods.

## 2. Tubes metallization

Tubes with different polymeric composites can be metalized by electroless deposition of a copper layer. As a first step, surface of the tubes was washed from excess or leftover materials that stay after chemical treatment and pre-production post-processing. The tube was connected to a homemade peristaltic pump, which maintains a high throughput flow of functional solutions through it. The cleaning cycle is applied at the end of the metallization process. DIW (Di Ionized Water) wash at room temperature was followed with methanol absolute dry wash at 50 °C for 5 min followed by rinsing with DIW. Then N,N-Dimethylformamide solution at 50 °C washed the tube for 5 min followed by rinsing with Ethanol then DIW. Etching to reduce the roughness on the tube walls by Chromo-Phosphoric-Sulfuric acid at 50 °C for 5 min was performed and followed by DIW rinsing. The next step is a sensibilization in a solution, containing $SnCl_2$-70 g/l and HCl – 40 ml/l for 30 min at room temperature, followed by DIW rinsing. Pd-activation for 60 min at room temperature with $PdCl_2$ 1 g/l solution, followed by DIW rinsing. Then copper solution 15 g/l, K-Na-tartrate 30 g/l $Na_2CO_3$ 10 g/l NaOH 40 g/l Formaldehyde 35%. Adjusting pH in the range 12.5 – 12.7 assuring metal layer formation properly at a proper rate compared to the reduction time of copper.

The surface roughness of copper layer was measured in Olympus LEXT OLS4100 laser scanning, providing a resolution of 10–20 nm. The quality of the surface was defined as the standard deviation of points on the surface from the mean position. The measurement was performed over $mm^2$-scale area. The surface roughness was estimated to be around 10 μm, while smaller areas of investigation were found to be as smooth as ±0.2 μm. It indicates that more accurate and repetitive surface cleaning can allow obtaining those numbers (corresponding to surface qualities of current commercially available 60 GHz hollow waveguide systems). The overall thickness of the metal layer, deposited on the inner side of the tube, is few microns (depending on copper solutions flow and duration), while the electromagnetic skin depth in copper at 10 GHz frequency is less than a micron. Fig. 2 (inset) shows a photo of a cut section of the metalized tube. The topographic image of the surface appears in the main figure (Fig. 2). The slant of the surface corresponds to the physical profile behavior, which can be almost perfectly fitted with a quadratic 2D polynomial. The quasi-periodic strips of the height profile (if projected on the flat landscape) are observed along the direction of the stream, which was induced inside the tube during the metallization process.

## 3. Extraction of waveguide loss - theory

Numerous techniques for extraction waveguide losses exist and tested on different realizations [26]. Overall energy losses of the whole system can be split into connectors and waveguide contributions. Hereafter, we are interested in the waveguide performance only, factoring out other effects. Waveguide losses themselves are spited into two categories: (i) absorption within metal parts and (ii) scattering on imperfections. The first factor sets a fundamental limit, which is specific to a particular geometry. Penetration of a mode into the metal is translated to the loss factor and can have analytical expressions, e.g. as in the case of circular crossection waveguide [27]. In our case, however, this theoretical limit is more than one order of magnitude below the extracted parameters, indicating that imperfections are the main contributing factor.

If waveguide losses are moderately low, multiple reflections of modes inside the structure are expected to emerge due to imperfect connectors' matching. General formalism of losses extraction in the case of multimode waveguide was reported in literature and summarized in e.g. [28], where waveguiding performances of ventilation systems are analyzed. Here, we employ relatively straightforward Fabry-Perot approach, as it provide the clear physical meaning to observed quantities and has a flexibility to introduce additional phenomenological parameters. In contrary to optical frequencies, where Fresnel coefficients define an etalon's

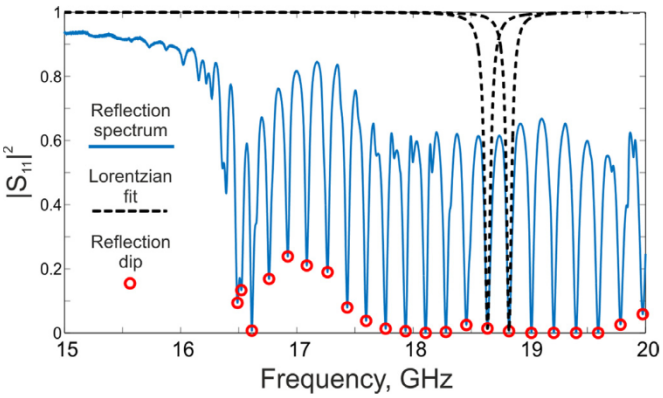


**Fig. 3.** Intensity reflection spectrum ($|S_{11}|^2$). Blue solid line – experimentally obtained reflection coefficient. Black dashed lines – Lorentzian fits for spectral dips. Red circles –spectral locations of dips.

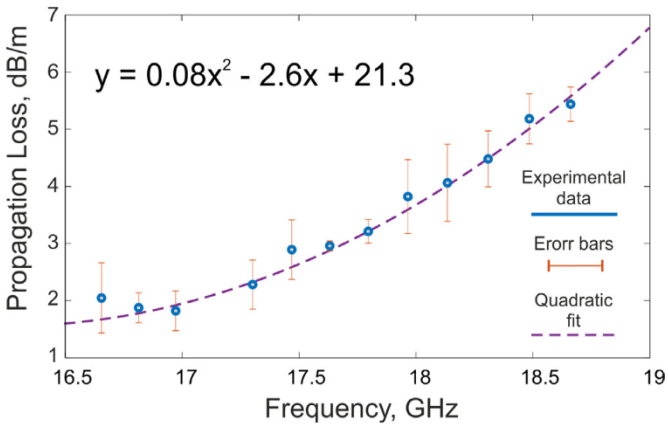


**Fig. 4.** Propagation losses as the function of frequency. Blue circles – experimental data, blue segments – error bars, dashed purple line – quadratic interpolation.

performance, RF connectors can have a nontrivial frequency response, which should be factorized. Several parameters for the subsequent analysis are defined hereafter. Finesse ($F$) of the waveguide cavity is approximated with:

$$F \approx \frac{c}{2L} \cdot \left(1 - \left(\frac{f_c}{f}\right)^2\right)^{-0.5} \cdot \frac{1}{(\delta f)}, \quad (1)$$

where 'c' is the speed of light, 'L' a length of the waveguide section, 'f' the operational frequency, '$f_c$' the waveguide cut-off frequency for the fundamental mode ($f_c = 1.8412c/(2\pi a)$, where 'a' is the waveguide radius), and '$\delta$f' the spectral with of a transmission peak (or reflection dip). Modal dispersion was assumed to be relatively weak and its modification between adjutant Fabry–Perot peaks was neglected.

Waveguide losses are calculated as (e.g. [29]):

$$\alpha_t L = \ln\left(\frac{\cos\left(\pi/F\right)}{1 - \sin\left(\pi/F\right)}\right) + const, \quad (2)$$

Where $\alpha_t = \alpha_l + \alpha_{con}$ is the total loss, separated into the intrinsic waveguide loss ($\alpha_l$) and connector's contribution ($\alpha_{con}$). Additive constant accounts for connectors' response and, in principle, can be frequency dependent too. Linear dependence on the waveguide length (L) allows performing straightforward regression to obtain the results, if several sections of a waveguide are available. This technique is frequently employed for obtaining more accurate results. In particular, transmission and reflection coefficients, measured for different waveguide sections, are used for loss retrieval. Here, we chose a realization, where the waveguide end-fire is shorten with a metal closure. This approach allows using one waveguide connector, simplifying the overall geometry. Consequently, the loss retrieval is based on $S_{11}$ spectra.

## 4. Extraction of waveguide loss - experiment

A metalized tube section was assessed for the waveguiding at the next stage. Standard SMA to waveguide connector was implemented on short sections of brass ducts (inner diameter of 11 mm), inserted into the metalized tube. End-fire of the tube was shorted with a brass closure. Reflection coefficient ($S_{11}$ parameters) of the system was retrieved with the VNA (N5232B PNA-L Microwave Network Analyzer) after performing standard calibration procedures (Fig. 3). Six waveguide sections (starting from 54 cm down to 49 cm with 1 cm step) were investigated. Flexible tube realization allows cutting off small waveguide sections, effectively shortening the structure (note, that any other existent waveguide layout will not allow such level of flexibility). Typical reflection spectrum for intensity appears in Fig. 3.

Several observations can be done by expecting the results. At first, the cut off frequency around 16 GHz can be clearly seen and it corresponds to the analytical expression. The reflection coefficient below this frequency does not reach unity, identifying internal loss of imperfectly matched connector. However, the mismatch is on the level of 5% for the intensity. Secondly, well-distinguished Fabry–Perot peaks with moderate Finesse are clearly seen and are almost equidistantly spread, if waveguide modal dispersion is properly accounted. Finally, the reflection does not approach its theoretical minimum $1/(1+(2F/\pi)^2)$ and is much higher. This phenomenon is attributed to additional loss within the dissipative and imperfectly matched connector. Several of the reflection dips are split into a pair of adjutant minima (e.g. the left marked dip on Fig. 3, where two nearby circles are closer than the free spectral range of the waveguide cavity). The structure has got a slight distortion during the metallization process and, as the result, additional reflections have been obtained. This can be prevented in the future by mechanical stabilization of the whole section during either pre- or post-processing. This statement was verified by additional manual mechanical deformation of the waveguide section.

Spectra, similar to the one from Fig. 3, were obtained for waveguide sections with different wavelength. Each spectral dip was fitted with a Lorentzian shape, Finesse was calculated according to Eq. (1) and loss factor was estimated by performing a linear regression (Eq. (2)). Results appear in Fig. 4 and demonstrate moderate losses, which increase with the frequency. This behaviour is reasonable and quite common to imperfectly smooth waveguides (e.g. [30]). Quadratic polynomial interpolation was found to be a reasonable phenomenological fit to the experimental data.

## 5. Bended waveguides

The distinctive advantage of the flexible waveguide platform is to support bending geometries - Fig. 5 (inset). Here, the overall length of the metalized tube is 1 m, while the bending radius is 16 cm. Fig. 5 shows the experimental results. Additional ~2 dB losses emerge from bending the structure.

## 6. Conclusions

A new platform for cheap and flexible high-frequency guiding was proposed and experimentally demonstrated. The

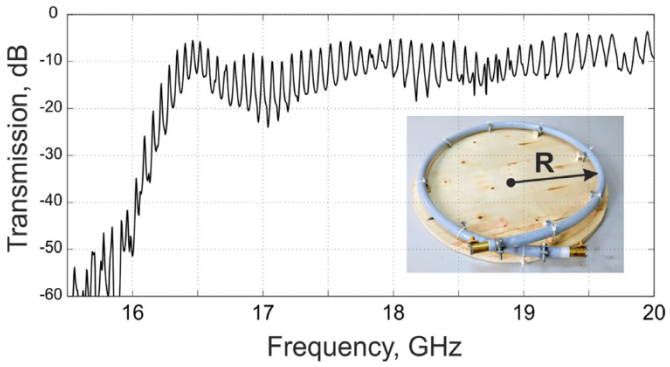


**Fig. 5.** Transmission trough bended metalized waveguide (Metalized polymer tube of 11 mm inner diameter, 1 m length, 16 cm bending radius).

principle is based on electroless plating of smooth bendable polymer tubes, whose inner surfaces undergo metallization. Highly conductive chemically deposited layers demonstrate properties, comparable with optically polished surfaces of conventional brass-based waveguide sections. As a result, efficient waveguiding at Ku-band was demonstrated. It is worth noting, that the developed methodology can be extended to higher frequencies, approaching 100 GHz and even higher. Standard waveguiding solutions demonstrate excessive losses at those frequencies. Furthermore, waveguide components become extremely expensive, preventing high-frequency RF technologies to replace existing widespread low GHz solutions (e.g. Wi-Fi and many others). Our solution might suggest a paradigm shift in this area.

## Acknowledgments

The research was supported in part by PAZY Foundation, Ministry of Science and Technology (project "Integrated 2D & 3D Functional Printing of Batteries with Metamaterials and Antennas"), and 3PEMS Ltd. The experimental part of research was partially supported by the Ministry of Education and Science of the Russian Federation (Project 3.1500.2017/4.6) and by Russian Foundation for Basic Research (project no. 18-79-10167).

## References

[1] Pozar DM. Microwave engineering. Wiley; 2012.
[2] Massoni E, Guareschi M, Bozzi M, Perregrini L, Tamburini UA, Alaimo G, Marconi S, Auricchio F, Tomassoni C. 3D printing and metalization methodology for high dielectric resonator waveguide microwave filters. In: *2017 IEEE MTT-S international microwave workshop series on advanced materials and processes for RF and THz applications (IMWS-AMP)*; 2017. p. 1–3.
[3] Ghazali MIM, Park KY, Gjokaj V, Kaur A, Chahal P. 3D printed metalized plastic waveguides for microwave components. *Int Symp Microelectron* 2017(1):000078–82 Oct. 2017.
[4] Rojas-Nastrucci EA, Nussbaum JT, Crane NB, Weller TM. Ka-band characterization of binder jetting for 3-D printing of metallic rectangular waveguide circuits and antennas. *IEEE Trans Microw Theory Tech* 2017.
[5] Weidenbach M, Jahn D, Rehn A, Busch SF, Beltrán-Mejía F, Balzer JC, Koch M. 3D printed dielectric rectangular waveguides, splitters and couplers for 120 GHz. *Opt Express* 2016;24(25):28968 Dec.
[6] Vogt DW, Anthony J, Leonhardt R. Metallic and 3D-printed dielectric helical terahertz waveguides. *Opt Express* 2015;23(26):33359 Dec.
[7] Zhang B, Linner P, Karnfelt C, Tarn PL, Sodervall U, Zirath H. Attempt of the metallic 3D printing technology for millimeter-wave antenna implementations. In: 2015 Asia-pacific microwave conference (APMC), 2; 2015. p. 1–3.
[8] Geterud EG, Bergmark P, Yang J. Lightweight waveguide and antenna components using plating on plastics. *7th Eur. conf. antennas propogation*; 2013.
[9] Zhu R, Marks D. Rapid prototyping lightweight millimeter wave antenna and waveguide with copper plating. IRMMW-THz 2015 - 40th international conference on infrared, millimeter, and terahertz waves; 2015.
[10] Huang Y, Wu H, Xiao L, Duan Y, Zhu H, Bian J, Ye D, Yin Z. Assembly and applications of 3D conformal electronics on curvilinear surfaces. *Mater Horizons* 2019.
[11] Liang M, Wu J, Yu X. 3D printing technology for RF and THz antennas. *IEEE* 2016;2:536–7 Jan.
[12] Ferrando-Rocher M, Herranz JI, Valero-Nogueira A, Bernardo B. Performance assessment of gap waveguide array antennas: CNC milling vs. 3D printing. *IEEE Antennas Wirel Propag Lett* 2018;1225 no. c, pp. 1–1.
[13] Al-Tarifi MA, Filipovic DS. On the design and fabrication of W-band stabilised–pattern dual-polarised horn antennas with DMLS and CNC. IET Microwaves Antennas Propag 2017;11(14):1930–5 Nov.
[14] Sonnerat F, Pilard R, Gianesello F, Le Pennec F, Person C, Gloria D. Innovative LDS antenna for 4G applications. IEEE 2013:2696–9 no. Eucap Apr.
[15] Friedrich A, Fengler M, Geck B, Manteuffel D. 60 GHz 3D integrated waveguide fed antennas using laser direct structuring technology. In: 2017 11th European conference on antennas and propagation, EUCAP 2017; 2017. p. 2507–10.
[16] Friedrich A, Geck B. On the design of a 3D LTE antenna for automotive applications based on MID technology. *Eur Microw Conf* 2013:640–3.
[17] Adams JJ, Slimmer SC, Malkowski TF, Duoss EB, Lewis JA, Bernhard JT. Comparison of spherical antennas fabricated via conformal printing: helix, meanderline, and hybrid designs. *IEEE Antennas Wirel Propag Lett* 2011;10:1425–8.
[18] Ahmadloo M. Design and fabrication of geometrically complicated multiband microwave devices using a novel integrated 3D printing technique. In: 2013 IEEE 22nd conference on electrical performance of electronic packaging and systems; 2013. p. 29–32.
[19] Liang M, Shemelya C, MacDonald E, Wicker R, Xin H. 3-D printed microwave patch antenna via fused deposition method and ultrasonic wire mesh embedding technique. *IEEE Antennas Wirel Propag Lett* 2015;14:1346–9.
[20] Ehrenberg I, Sarma S, Steffeny T, Wuy B-I. Fabrication of an X-Band conformal antenna array on an additively manufactured substrate. In: 2015 IEEE International symposium on antennas and propagation & USNC/URSI national radio science meeting; 2015. p. 609–10.
[21] Wu B-I, Ehrenberg I. Ultra conformal patch antenna array on a doubly curved surface. In: 2013 IEEE international symposium on phased array systems and technology; 2013. p. 792–8.
[22] Filonov D, Kolen S, Shmidt A, Shacham-Diamand Y, Boag A, Ginzburg P. Volumetric 3D-printed antennas, manufactured via selective polymer metallization. *Phys Status Solidi - Rapid Res Lett* 2019. Feb.
[23] Mirzaee M, Noghanian S, Chang I. Low-profile bowtie antenna with 3D printed substrate. *Microw Opt Technol Lett.* 2017;59(3):706–10 Mar.
[24] Shemelya C, Zemba M, Liang M, Yu X, Espalin D, Wicker R, Xin H, MacDonald E. Multi-layer archimedean spiral antenna fabricated using polymer extrusion 3D printing. *Microw Opt Technol Lett* 2016;58(7):1662–6 Jul.
[25] Parsons P, Mirotznik M, Pa P, Larimore Z. Multi-material additive manufacturing of embedded low-profile antennas. *Electron Lett* 2015;51(20):1561–2 Oct.
[26] РБ МВВВаганов, РФ Матвеев. Многоволновые волноводы со случайными нерегулярностями. Советское радио; 1972.
[27] Balanis CA. Advanced engineering electromagnetics. Wiley; 1989.
[28] P.V. Nikitin, D.D. Stancil, O.K. Tonguz, A.E. Xhafa, A.G. Cepni, and D. Brodtkorb, "RF propagation in an HVAC duct system : impulse response characteristics of the channel." 2002.
[29] Tittelbach G, Richter B, Karthe W. Comparison of three transmission methods for integrated optical waveguide propagation loss measurement. *Pure Appl Opt J Eur Opt Soc Part A* 1993;2(6):683–700 Nov.
[30] M. D'Auria, W.J. Otter, J. Hazell, B.T.W. Gillatt, C. Long-Collins, N.M. Ridler, and S. Lucyszyn, "3-D printed metal-pipe rectangular waveguides," undefined, 2015.